DOI: 10.1002/chem.200801724

Self-Assembled Heavy Lanthanide Orthovanadate Architecture with Controlled Dimensionality and Morphology

Liwu Qian, Jun Zhu, Zhu Chen, Yicai Gui, Qiang Gong, Yanping Yuan, Jiantao Zai, and Xuefeng Qian*[a]

Abstract: Nearly monodisperse YVO_4 architectures with persimmon-like, cube-like and nanoparticle shapes have been synthesised on a large scale by means of a complexing-agent-assisted solution route. The shape and size of these as-prepared architectures can be tuned effectively by controlling the reaction conditions, such as reaction time, the molar ratio of complexing agent/Y^{3+} and different complexing agents. As a typical morphology, the growth process of monodisperse nanopersimmons has been examined. To extend this method, other $LnVO_4$ (Ln = Ce, Gd, Dy, Er) complexes with well-defined shape and dimensionality can also be achieved by adjusting different rare earth precursors. Further studies reveal that the morphology of the as-synthesised lanthanide orthovanadate is determined mainly by the interaction between rare earth ion and the complexing agent. Ultraviolet (UV) absorption and photoluminescence spectra show that the optical properties of YVO_4 nanopersimmons are relevant to their size and shape. This work sheds some light on the design of well-defined complex nanostructures, and explores the potential applications of the as-synthesised architectures.

Keywords: hydrothermal synthesis · lanthanides · nanostructures · self-assembly · vanadium

Introduction

In recent years, the design and synthesis of inorganic nanostructures with well-defined size and morphology have attracted considerable attention, because the dimensional and structural characteristics of these materials endow them with a wide range of potential applications.[1] In particular, the fabrication of hierarchical and complex nano-/microstructures that assemble from nanoparticles, nanorods, nanoribbons or nanobelts as building blocks at different levels have been proposed and partially realised in recent years.[2–5] These novel architectures should facilitate a deeper understanding of the "bottom-up" approaches and offer opportunities in searching for exciting new properties of materials, and be useful for fabricating functional nanodevices, and so forth.[5–7] Until now, some kinds of compounds or materials, such as metal oxides,[8] sulfides,[7,9] hydrates[10] and other compounds,[11] have been synthesised with controlled hierarchical/complex morphologies by various methods. In these fabrications, the growth habit of crystals always plays an important role in determining the final morphology; meanwhile, the complexing agent or surfactant is also used for tailing the crystal growth dynamically. Moreover, the use of a complexing agent affords the possibility of breaking the limitation of crystal growth habit and results in various hierarchical/complex morphologies. Therefore, to extend the synthesis of inorganic hierarchical/complex morphologies and to deepen the comprehension of crystal growth behaviour, it is necessary to choose suitable complexing agents or surfactants for preparing inorganic hierarchical/complex morphologies with uniform size. Herein, trisodium citrate (Na_3cit), sodium tartrate (Na_2tar) and sodium malate (Na_2mal) are chosen to control the synthesis of rare earth orthovanadates, and Na_3cit and Na_2tar prove to useful for preparing hierarchical/complex morphologies.

As a series of important functional inorganic materials, rare earth orthovanadates have been extensively studied and employed in various fields including catalysts,[12] polarisers,[13] laser host materials[14] and phosphors.[15] Stimulated by both the promising applications and the interesting properties, much attention has been directed to the controlled

[a] Dr. L. Qian, Dr. J. Zhu, Z. Chen, Y. Gui, Dr. Q. Gong, Dr. Y. Yuan, Dr. J. Zai, Prof. X. Qian
School of Chemistry and Chemical Technology
State Key Laboratory of Metal Matrix Composites
Shanghai Jiao Tong University, Shanghai 200240 (P. R. China)
Fax: (+86) 21-5474-1297
E-mail: xfqian@sjtu.edu.cn

Supporting information for this article is available on the WWW under http://dx.doi.org/10.1002/chem.200801724.

synthesis of rare earth orthovanadates with different shapes, and the investigation of their size/shape-dependent properties in the past several years, especially in nanorods/nanowires[16] and nanoparticles.[17] Recently, polyhedral YVO_4 nanocrystals also have been prepared by the wet chemical synthesis process.[18] Nevertheless, to the best our knowledge, the synthesis of monodisperse YVO_4 complex architectures with uniform size and morphology has seldom been reported. On the other hand, the shape, crystalline structure and size of YVO_4 are important elements in determining its physical and chemical properties. Therefore, to control the shape and size of YVO_4 complex, it is necessary to understand the relationship between the intrinsic crystal structure of YVO_4 and the kinetic factors employed during the synthetic course, such as the reaction time, the molar ratio of the complexing agent/Y^{3+} and different complex agents.[19] Furthermore, this shape control of YVO_4 crystals will, to some extent, give insights into the crystallisation behaviour on a nano- or microsize scale owing to the traditional lack of understanding of the growth history and shape evolution process.

In this paper, nearly monodisperse YVO_4 particles with nanopersimmon, nanocube and nanoparticle shape have been successfully prepared through a complexing-agent-assisted hydrothermal approach. The shape and dimensionality of the obtained YVO_4 architectures can be controlled by adjusting the reaction time, the molar ratio of complexing agen/Y^{3+} and different complexing agents, for example, Na_3cit, Na_2tar and Na_2mal. Because of the different interactions between the rare earth ion and the complexing agent, it is interesting to find that the as-synthesised heavy rare-earth orthovanadates $ErVO_4$ and $DyVO_4$ have similar morphological variation to YVO_4 through the use of different complexing agents under similar reaction conditions. Whereas, for the as-obtained light rare-earth orthovanadates $CeVO_4$ and $GdVO_4$, the complexing agents have no evident effect on their morphology and only nanoparticles are obtained. Pore-size distribution analysis results indicate that there are mesopores (2–4 nm) in the nanopersimmon and macropores (10–50 nm) in the nanocube. UV absorption and photoluminescence spectra show that the optical properties of YVO_4 nanopersimmons are relevant to their sizes and shapes.

Results and Discussion

Synthesis of YVO_4 architectures with nanopersimmon and nanocube shapes: $LnVO_4$ (Ln = Y, Dy, Er, Ce, Gd) have been synthesised by means of a complexing-agent-assisted solution route. The detailed reaction parameters and corresponding results are summarised in Table 1. The scanning electron microscopy (SEM) image of sample 6 is shown in Figure 1; uniform and persimmon-like YVO_4 hierarchical structures are obtained on a large scale (Figure 1a). There is a concave dip in each centre of the YVO_4 architecture. The average size of the as-prepared product is about 940 nm in diameter and 470 nm in thickness. The rough surface and evident boundaries of the obtained 2D persimmon-like patterns indicate that an individual YVO_4 architecture is composed of many smaller nanoplates (Figure 1b and 1c), and these original nanoplates are self-assembled into an integrated structure along the longitudinal axis direction through face-by-face attachment. This organisation is similar to the

Table 1. Reaction conditions and corresponding morphologies of the as-synthesised $LnVO_4$.[a]

Sample	Agent	Molar ratio	t [h]	Product	Morphology
1	Na_3cit	0:1	24	YVO_4	nanoparticles
2	Na_3cit	1:1	24	YVO_4	nanoparticles
3	Na_3cit	2:1	1	YVO_4	nanodisks
4	Na_3cit	2:1	6	YVO_4	nanodisks
5	Na_3cit	2:1	12	YVO_4	nanopersimmons
6	Na_3cit	2:1	24	YVO_4	nanopersimmons
7	Na_3cit	3:1	24	YVO_4	nanopersimmon and stacks of nanopersimmon
8	Na_3cit	4:1	24	YVO_4	stacks of nanopersimmon
9	Na_2tar	2:1	24	YVO_4	nanocubes
10	Na_2mal	2:1	24	YVO_4	nanoparticles
11	Na_3cit	2:1	24	$DyVO_4$	nanopersimmons
12	Na_2tar	2:1	24	$DyVO_4$	nanocubes
13	Na_2mal	2:1	24	$DyVO_4$	nanoparticles
14	Na_3cit	2:1	24	$ErVO_4$	nanopersimmons
15	Na_2tar	2:1	24	$ErVO_4$	nanocubes
16	Na_2mal	2:1	24	$ErVO_4$	nanoparticles
17	Na_3cit	2:1	24	$CeVO_4$	nanoparticles
18	Na_2tar	2:1	24	$CeVO_4$	nanoparticles
19	Na_2mal	2:1	24	$CeVO_4$	nanoparticles
20	Na_3cit	2:1	24	$GdVO_4$	nanoparticles
21	Na_2tar	2:1	24	$GdVO_4$	nanoparticles
22	Na_2mal	2:1	24	$GdVO_4$	nanoparticles

[a] All samples were prepared by hydrothermal process at 140 °C with $Ln(NO)_3{\cdot}6H_2O$ (Ln = Y, Dy, Er, Ce, Gd) as precursors.

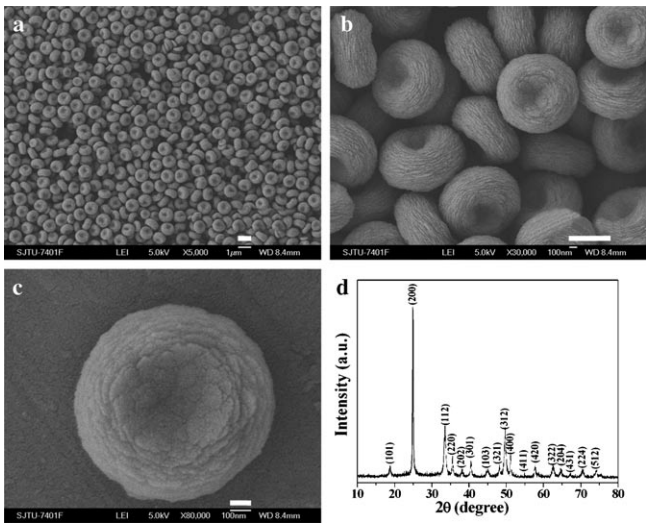

Figure 1. a) Low-magnification SEM image of monodisperse YVO_4 nanopersimmons obtained with 2:1 molar ratio of cit^{3-}/Y^{3+} at 140 °C for 24 h; scale bar 1 μm; b) enlarge SEM image of YVO_4 nanopersimmons; scale bar 500 nm; c) SEM image of an individual YVO_4 nanopersimmon; scale bar 100 nm; d) XRD pattern of the YVO_4.

ZnO "parent" nanorod self-assembled from smaller nanorods.[8c] Figure 1d shows the typical X-ray diffraction (XRD) pattern of the YVO_4 samples. The pattern fits well with the tetragonal (zircon) type YVO_4 (space group: $I41/amd$) with lattice constants $a=b=7.123$ Å and $c=6.292$ Å (JCPDS 72-0861). No peaks of any other phases or impurities can be detected, indicating its pure phase.

The morphology of YVO_4 architecture was further investigated by high-resolution transmission electron microscopy (HRTEM). The bright field transmission electron microscopy (TEM) image of an individual YVO_4 persimmon clearly shows that the obtained YVO_4 is in spherical shape. The different contrast between the central and fringe part of an individual architecture also implies the concave dip existing in the centre of products (Figure 2a). The corresponding

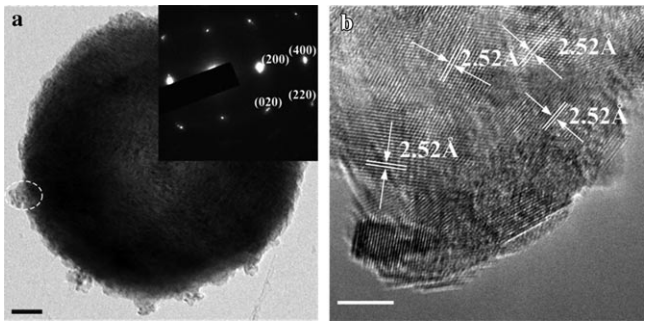

Figure 2. a) TEM image of an individual YVO_4 nanopersimmon, the inset gives the corresponding SAED; scale bar 100 nm; b) HRTEM image of the YVO_4 nanoplates; scale bar 5 nm.

selected-area electron diffraction (SAED) pattern taken from discretional nanoplate indicates that the assembled nanoplate has a well-defined single-crystalline structure (inset of Figure 2a). The HRTEM image in Figure 2b further reveals the single-crystal characteristic structure of nanoplates. The 2.52 Å spacing of crystallographic planes corresponds to the (220) lattice fringe of YVO_4, indicating the growth along [001] direction was confined, and it grew preferentially along the [100] and [010] directions; nanoplates were then obtained.[17a–b] It can also be observed that the original plates are about 10 nm in size. This feature gives evidence that YVO_4 nanopersimmons are stacked through "oriented attachment"[20–22] of small nanoplates along the [001] direction.

To control the size and morphology of YVO_4 architecture, the influence of reaction time, the molar ratio of Na_3cit/Y^{3+} and different complexing agents was investigated. It is found that the size of the obtained monodisperse YVO_4 architecture can be easily tuned by the reaction time. As shown in Figure 3, the as-synthesised YVO_4 are uniform architectures with 300 nm in diameter and 50 nm in thickness after the reaction was carried out for 1 h (sample 3; Figure 3a). If the reaction time was prolonged to 6, 12 or 24 h (sample 4–6), uniform and monodisperse architecture with a "disk" shape was still obtained. Meanwhile, the corresponding diameter is

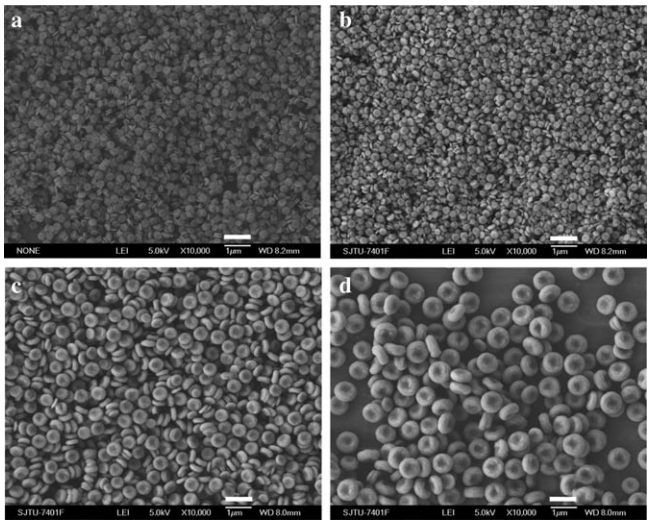

Figure 3. SEM images of YVO_4 obtained with 2:1 molar ratio of cit^{3-}/Y^{3+} at 140 °C for different reaction time: a) 1, b) 6, c) 12 and d) 24 h; scale bars 1 μm.

400, 520 and 940 nm, respectively, and the thickness increases from 50 to 470 nm (Figure 3b–d). These images clearly demonstrate the shape evolution of the obtained products from thick nanodisk to nanopersimmon.

On the other hand, the molar ratio of cit^{3-}/Y^{3+} also has great influence on the morphology evolution of YVO_4. Quasi-spheres were obtained if the molar ratio of cit^{3-}/Y^{3+} was lower than two (samples 1 and 2; Figure 4a,b). The average size of the irregular nanoparticles is about 17 and 28 nm, respectively. The organised structures form short pillars, assembled from many nanoplates through face-to-face stacking, and are obtained at the cit^{3-}/Y^{3+} molar ratio of 3:1 (sample 7; Figure 4c). The length of the aggregated pillar extended when the cit^{3-}/Y^{3+} molar ratio was increased to 4:1 (sample 8; Figure 4e). However, the diameter of the pillar decreased from 860 to 600 nm. It is observed that the organised units (nanodisks or nanopersimmons) are secondary structural units of the original nanoplates with 27 nm in thickness (Figure 4d and 4f), and these original nanoplates also organised through face-to-face way to form nanopersimmons or the pillar structure. In the present system, the molar ratio of cit^{3-}/Y^{3+} is undoubtedly vital in the morphologies and self-assemble of YVO_4 microstructure.

A plausible process for the self-assembly of YVO_4 nanopersimmons is proposed (Figure 5). It is known that Na_3cit is a rich source of COO^- ions and can form complexes with Y^{3+} ion through coordination interaction.[23] When Na_3cit is added into the solution, it can coordinate with Y^{3+} ion to form the intermediate complex of $[Y(cit)_2]$, greatly decreasing the free Y^{3+} ion concentration in solution. Such a low Y^{3+} ion concentration leads to a relatively slow reaction rate and facilitates the oriented growth of YVO_4 nanocrystals in the view of the dynamic process. When $[Y(cit)_2]$ is attacked by VO_4^{3-}, the active (001) facet of tetragonal YVO_4 is restricted by the released cit^{3-} ions.[17a–b] Thus the crystal

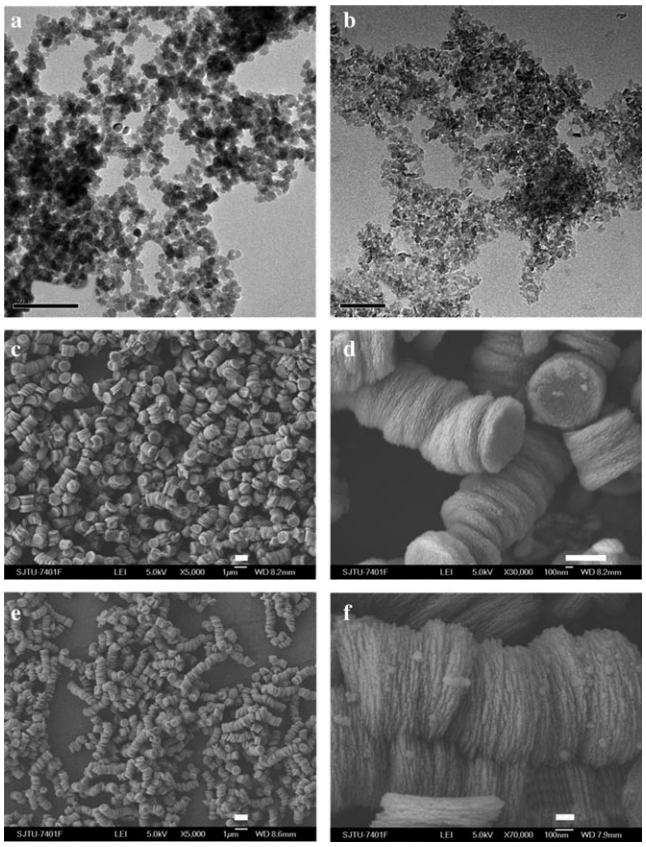

Figure 4. SEM images of the products obtained at 140 °C for 24 h with different molar ratio of cit^{3-}/Y^{3+}: a) 0:1, scale bar 100 nm; b) 1:1 scale bar 100 nm;, c) 3:1, scale bar 1 μm; d) 3:1, scale bar 500 nm; e) 4:1, scale bar 1 μm; f) 4:1, scale bar 100 nm.

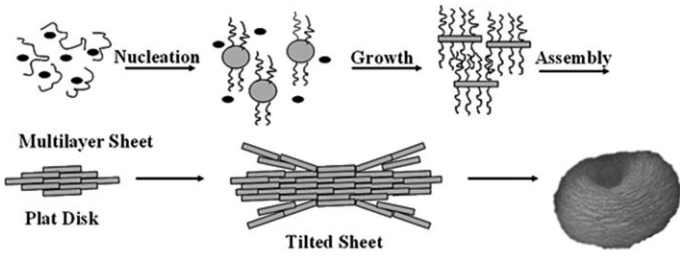

Figure 5. Schematic illustration of the growth process of YVO_4 nanopersimmon.

growth along [001] direction is confined, and it grows preferentially along [100] and [010] directions. This kinetic control leads to the formation of the original nanoplates with the preferential growth directions. (The YVO_4 nanoplates capped by cit^{3-} are easily soluble in water and difficult to collect by centrifugal separation.) As evidenced by TEM and SAED results, the assembled nanopersimmons are constructed by tiny nanoplates, with their top/bottom faces covered by {001} planes. Then these initially formed nanoplates assemble in edge-to-edge and layer-by-layer stacking style due to the hydrogen bond and electrostatic effects of cit^{3-} ions. Subsequently, the curved nanostructures can be formed with the help of the cit^{3-} ions.[11a,b] This interaction can also be confirmed by the infrared (IR) spectrum (see Figure S1 in the Supporting Information). Meanwhile, the aggregated nanoplates still undergo the Ostwald ripening process at the cost of the smaller nanoparticles, and the size of the as-obtained monodisperse nanopersimmons increases with the reaction time. Based on the above results, it is reasonable to believe that Na_3cit plays double roles in the reaction. One is to serve as chelating ligand to form a stable complex with Y^{3+} and further kinetically control the reaction rate, and the other is to act as capping agent to affect the facet growth and their assembly. However, if the molar ratio of cit^{3-}/Y^{3+} is low to 2:1, the released Y^{3+} ion concentration from the complex is higher, because of low coordination number of cit^{3-} chelation with Y^{3+}. This accelerates the nucleation process of YVO_4 and leads to the aggregation of YVO_4 nuclei before preferential growth during the hydrothermal process, so YVO_4 nanoparticles are formed.[11a] If the molar ratio of cit^{3-}/Y^{3+} is increased to 3:1, a low free Y^{3+} ion concentration dissociated from the complex results in a relatively slow reaction rate and facilitates the preferential growth of YVO_4. Furthermore, the stronger electrostatic effects of the nanoplates capped by the greater amounts of cit^{3-} ions will lead the nanoplates to self-assemble further into organised pillar structures. A large number of nanoplates are self-assembled into longer pillar structure with the molar ratio of cit^{3-}/Y^{3+} increasing to 4:1. Based on the above experiment results, it is natural to deduce that the formation of YVO_4 hierarchical structures by self-assembly is a cooperative effect of the cit^{3-}/Y^{3+} molar ratio, reaction rate and inherent electronic nature of complexing agent.

To further explore the real factors affecting the morphologies or the self-assemble styles of YVO_4, different complexing agents were also studied (see Figure S2 in the Supporting Information). It is found that nanocubes rather than nanopersimmons are obtained when Na_2tar is used as a complexing agent under similar reaction conditions (sample 9; Figure 6a). The obtained products also have uniform morphologies and can be prepared in large quantity. However, the obtained products have cubic shapes, about 1000 nm in length and 450 nm thick. It is observed that the nanocube is also composed of numerous nanoplates with an average size about 60 nm, and there is also a shallow concave dip in the each face of the nanocube (Figure 6c). The densely packed nanoplates make the nanocube surface rough and corrugated. The XRD result indicates that the obtained products are pure tetragonal YVO_4 (Figure 6d). It is worth mentioning that these YVO_4 nanocubes are sufficiently stable even though they are ultrasonically treated for long time. On the other hand, no morphology change was observed even when the molar ratio of tar^{2-}/Y^{3+} was increased to 3:1.

A typical TEM image of YVO_4 nanocubes shows that they are formed by the self-assemble of nanoplates, and the original units form in square shape with an evident right angle (Figure 7a). The SAED pattern (inset of Figure 7a) of a piece of the nanoplate reveals its single-crystalline nature.

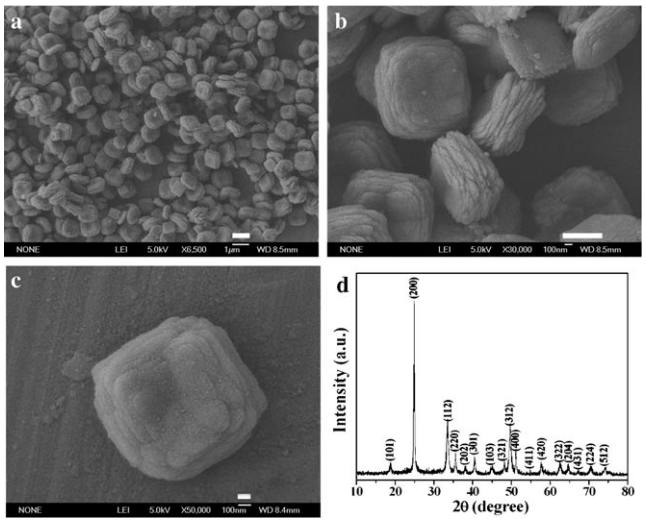

Figure 6. a) Low-magnification SEM image of monodisperse YVO_4 nanocubes obtained with 2:1 molar ratio of tar^{2-}/Y^{3+} at 140 °C for 24 h; scale bar 1 μm; b) enlarged SEM image of YVO_4 nanocubes; scale bar 500 nm; c) SEM image of an individual YVO_4 nanocube; scale bar 100 nm; d) XRD pattern of YVO_4 nanocubes.

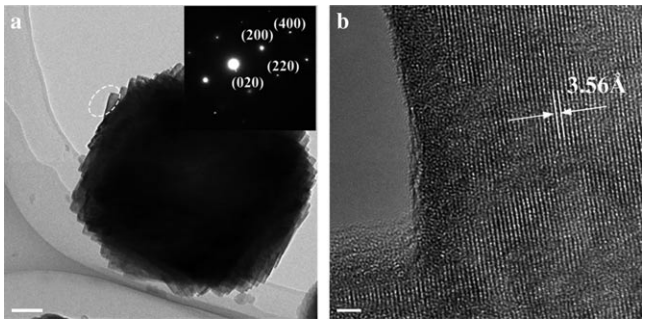

Figure 7. a) TEM image of an individual YVO_4 nanocube, the inset gives the corresponding SAED; scale bar 100 nm; b) HRTEM image of YVO_4 nanoplate, scale bar 2 nm.

The 3.56 Å lattice interplanar spacing taken from the part of an individual nanoplate (Figure 7b) corresponds to the (200) plane of tetragonal YVO_4. This phenomenon can also be explained by the fact the growth along the [001] direction was restricted by the additive tar^{2-} ions, resulting in the formation of YVO_4 nanoplates.[17a–b] However, only irregular nanoparticles instead of specific architectures are obtained when Na_2mal was used as the complexing agent under similar reaction condition, and the size of the obtained particles is about 15–25 nm (sample 10; Figure 8a).

From the above controlled experiments, it is found that the complexing agents have great effects on the morphologies of the products. It is evident that Na_3cit has three carboxyl and two hydroxyl groups, the Na_2tar molecule possess two carboxyl and two hydroxyl groups and the Na_2mal molecule has two carboxyl and one hydroxyl groups (see Figure S2 in the Supporting Information). Therefore, among the Y^{3+} complexes of these three ligands, the complex of

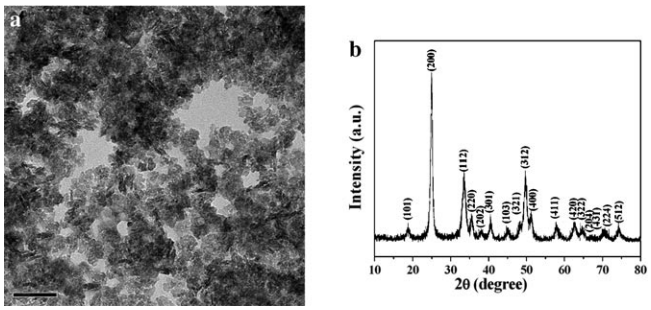

Figure 8. a) TEM image of YVO_4 nanoparticles obtained with 2:1 molar ratio of mal^{2-}/Y^{3+} at 140 °C for 24 h; scale bar 100 nm; b) XRD pattern of YVO_4 nanoparticles.

Y^{3+} chelated with Na_2mal shows the least steric hindrance for VO_4^{3-} attack, which facilitates the formation of YVO_4 nanoparticles without the preferential growth direction.[17a] On the other hand, our results reveal that Na_3cit and Na_2tar can effectively control the crystal growth of YVO_4 nanoplate and direct these nanoplates to assemble hierarchical/complex morphologies, because of their inherent steric effect and electric character. With respect to the cit^{3-} ion, the charge of tar^{2-} ion absorbing on the layer is not enough to form pillar structures. As to YVO_4 morphology evolution from nanopersimmon to nanocube by using Na_3cit and Na_2tar as the complexing agent, respectively, it is believed that the different framework formed by the coordination ligand with the Y^{3+} ion plays an important role in determining the final shape of product. Of course, these factors need to be further studied in detail.

The nitrogen adsorption–desorption isotherms and porosity of the obtained architectures were further investigated for the YVO_4 nanopersimmons and nanocubes. As can be seen in Figure 9, the pore size of the nanopersimmons (inset of Figure 9 top) is distributed in the 2–4 nm range, and the pore size of the nanocubes (inset of Figure 9 bottom) is in the range of 10–80 nm, but is concentrated at 13 nm. The specific surface area of YVO_4 nanopersimmons and nanocubes is 73.87 and 33.04 $m^2 g^{-1}$, respectively. These mesopores or macropores could endow these as-prepared hierarchical structures with some novel potential applications.

Synthesis of $CeVO_4$, $GdVO_4$, $DyVO_4$, $ErVO_4$: The stability of complex may be influenced by the sufficient correspondence of the bite between the yttrium ion and the complexing agent. The series of rare-earth elements is frequently divided into two groups based on the atomic weight and chemical properties. The "light" rare earths consist of elements with atomic number 57 to 63. The "heavy" rare earths consist of elements 64–71, as well as scandium and yttrium because of their similar chemical behaviour. The ionic radius of rare earth elements decreases from atomic number 57 to 71, and the ionic radius of Y^{3+} lies between that of Dy^{3+} and Ho^{3+}.[24] In this paper, $CeVO_4$ (samples 17–19), $GdVO_4$ (samples 20–22), $DyVO_4$ (samples 11–13) and $ErVO_4$ (samples 14–16) have also been synthesised under similar reaction conditions

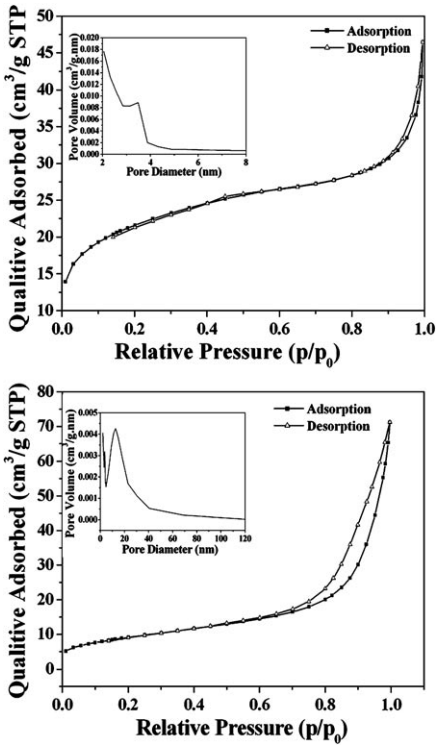

Figure 9. Typical N_2 gas adsorption–desorption isotherms of YVO_4 monodisperse architecture: Top: nanopersimmon; bottom: nanocubes. The inset is the corresponding pore-size distribution.

with these three complexing agents, respectively. It is found that $DyVO_4$ and $ErVO_4$ have similar morphology variation to that of YVO_4 (Figure 10) and only nanoparticles are obtained for $CeVO_4$ and $GdVO_4$ (see Figure S4 in the Supporting Information). In spite of a larger ionic radius, Ce^{3+} and Gd^{3+} can be chelated with these three complexing agents to form different complexes that show relatively smaller steric repulsion for the attack of VO_4^{3-} ions, resulting in the formation of nanoparticles before preferential growth.[17b] Owing to the lanthanide contraction, there is a little morphology variation among the as-obtained different lanthanide orthovanadates because of their individual properties. Therefore, the assembly of $LnVO_4$ hierarchical architectures is a complicated process affected by several factors, including reaction time, the molar ratio of the complexing agent/Ln^{3+}, different complexing agents and precursors. These results show the shape evolution of lanthanide orthovanadate is determined mainly by interaction between rare earth ion and the complexing agent.

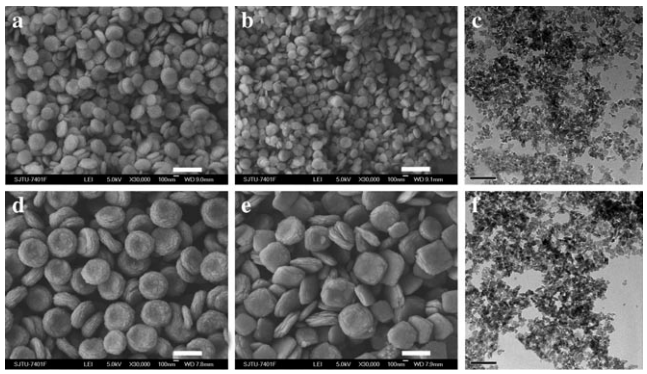

Figure 10. a)and b) Low-magnification SEM image (scale bars 500 nm) and c) TEM image (scale bar 100 nm) of $DyVO_4$ samples obtained with 2:1 molar ratio of cit^{3-} (tar^{2-} or mal^{2-})/Dy^{3+} at 140 °C for 24 h; d) and e) Low-magnification SEM image (scale bars 500 nm) and f) TEM image (scale bar 100 nm) of $ErVO_4$ samples obtained with 2:1 molar ratio of cit^{3-} (tar^{2-} or mal^{2-})/Er^{3+} at 140 °C for 24 h.

Optical properties of YVO_4 nanopersimmons: YVO_4 is an important optical host material, but few reports are available on the intrinsic photoluminescence properties such nanomaterials. In this work, the photoluminescence properties of YVO_4 nanopersimmons of various sizes were studied; typical adsorption spectra of YVO_4 nanocrystals obtained at different times are presented in Figure 11 (top). The spectral characteristics of YVO_4 nanocrystals are similar in the UV region, but a little difference in adsorption. Compared with other YVO_4 nanopersimmons obtained at different time, YVO_4 nanopersimmons obtained at 1 h shows strongest adsorption peak at 270 nm. In the UV region, the broad band between 270–280 nm is attributed to charge transfer from the oxygen ligands to the central vanadium atom inside the VO_4^{3-} ion.[17a] The photoluminescence emission spectra of

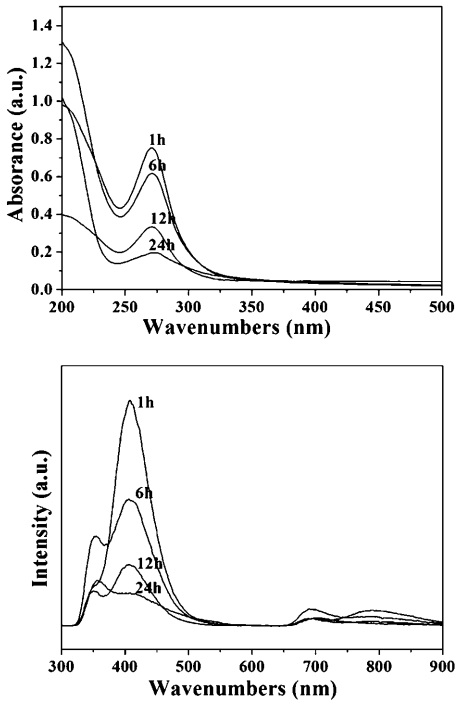

Figure 11. UV spectra (top) and photoluminescence spectra (bottom) of the YVO_4 monodispersed nanopersimmon obtained at different time.

YVO_4 nanopersimmons are shown in Figure 11 (bottom) excited by 270 nm wavelength light, and they have similar emission spectra exhibiting bands at 354, 406, 695 and 791 nm, respectively. The adsorption and emission character of YVO_4 nanopersimmons obtained at 6 h is similar to that of regular colloid of YVO_4 particles. In general, the photoluminescence emission intensity of nanocrystals increases with improving crystallinity.[11h] However, it is interesting to find that the relative intensity of photoluminescence spectra in our experiments reduces with the increase in reaction time and the size of nanocrystals; the ratio of photoluminescence of samples obtained at different time also gradually decreases. As to these abnormal phenomena, it might be due to the diffusion and the unstable suspended colloid in water because of the size of YVO_4 nanopersimmons increasing with the reaction time prolonging. The factors also need to be explored in more detail in the future.

Conclusion

In summary, nearly monodisperse YVO_4 nanopersimmons, nanocubes and nanoparticles can be synthesised by a complexing-agent-assisted hydrothermal approach. The obtained nanopersimmons and nanocubes are composed of many nanoplates, and the shape and dimensionality of the obtained architectures can be controlled by adjusting the reaction time, the molar ratio of the complexing agent/Y^{3+} and different complexing agents, for example, Na_3cit, Na_2tar and Na_2mal. The optical properties of YVO_4 nanopersimmons are relevant to their size and shape. This method can be extended to synthesise other rare-earth orthovanadates, and their size and morphology can also be controlled effectively. Further studies reveal that the morphology of the as-synthesised $LnVO_4$ is determined mainly by the interaction between rare-earth ion and the complexing agent. This work may present a way for the morphology-controlled synthesis of other inorganic materials.

Experimental Section

Synthesis of rare earth orthovanadate $LnVO_4$ (Ln=Y, Ce, Gd, Dy, Er): YVO_4 was synthesised by a hydrothermal process. $Y(NO_3)_3{\cdot}6H_2O$ (0.56 mmol) was dissolved into an aqueous solution of Na_3cit ($C_6H_5Na_3O_7{\cdot}2H_2O$) (28 mL, 1.12 mmol, 0.04 mol L^{-1}). The solution was stirred at room temperature for 10 min to form a yttrium citrate complex. Then $Na_3VO_4{\cdot}12H_2O$ (0.56 mmol) was added into the solution. After being stirred for 10 min, the clear and colourless solution was transferred into a 35 mL Teflon-lined autoclave (filled up to 80% of its total volume), and the autoclave was heated at 140 °C for 24 h. Then autoclave was allowed to cool to room temperature. The obtained samples were collected after being centrifugally separated at 3500 rpm for 20 min and were washed with deionised water and dried at 60 °C in air. The detailed reaction parameters and corresponding results are summarised in Table 1.

Characterisation: The phase of the as-prepared products was characterised on powder XRD (Shimadzu XRD-6000) equipped with a $Cu_{K\alpha}$ radiation source ($\lambda = 1.5418$ Å) at a scanning rate of 6° min^{-1} (2θ from 10° to 80°), X-ray tube voltage and current were set at 40 kV and 30 mA, respectively. The morphology and crystal lattice of the samples were characterised by TEM (JEOL, JEM-100CX, with an accelerating voltage of 100 kV), HRTEM (JEOL, JEM-2100F, with an accelerating voltage of 200 kV) and field-emission scanning electron microscopy (FE-SEM; JEOL, JSM-6700F with an accelerating voltage of 5 kV), respectively. Fourier transformation infraFTIR spectra were recorded on Perkin–Elmer Paragon 1000FT-IR Spectrometer. Nitrogen adsorption–desorption measurements were conducted at 77.73 K on a Micromeritics ASAP 2010 analyser, and the BET (Brunauer–Emmett–Teller) surface area was estimated from adsorption data. The UV and photoluminescence spectra were investigated on Perkin–Elmer Lambda 20/2000 UV spectrophotometer and Perkin–Elmer LS50B photoluminescence spectrophotometer by dispersing samples in deionised water.

Acknowledgement

The work described here was supported by the National Science Foundation of China (No F20671061), the Program for New Century Excellent Talents of Education Ministry of China, and National Basic Research Program of China (2009CB930400 and 2007CB209705).

[1] a) Z. W. Pan, Z. R. Dai, Z. L. Wang, *Science* **2001**, *291*, 1947–1949; b) D. Li, J. T. McCann, Y. N. Xia, *Small* **2005**, *1*, 83–86; c) Y. N. Xia, P. D. Yang, Y. G. Sun, Y. Y. Wu, B. Mayers, B. Gates, Y. D. Yin, F. Kim, H. Q. Yan, *Adv. Mater.* **2003**, *15*, 353–389.

[2] T. D. Ewers, A. K. Sra, B. C. Norris, R. E. Cable, C. H. Cheng, D. F. Shantz, R. E. Schaak, *Chem. Mater.* **2005**, *17*, 514–550.

[3] H. G. Yang, H. C. Zeng, *Angew. Chem.* **2004**, *116*, 6056–6059; *Angew. Chem. Int. Ed.* **2004**, *43*, 5930–5933.

[4] X. Y. Chen, X. Wang, Z. H. Wang, X. G. Yang, Y. T. Qian, *Cryst. Growth Des.* **2005**, *5*, 347–350.

[5] a) Z. Q. Li, Y. Ding, Y. J. Xiong, Q. Yang, Y. Xie, *Chem. Commun.* **2005**, 918–920; b) Z. Q. Li, Y. Ding, Y. J. Xiong, Y. Xie, *Cryst. Growth Des.* **2005**, *5*, 1953–1958.

[6] a) S. Mann, *Angew. Chem.* **2000**, *112*, 3532–3548; *Angew. Chem. Int. Ed.* **2000**, *39*, 3392–3406; b) A. Bigi, E. Boanini, D. Walsh, S. Mann. *Angew. Chem.* **2002**, *114*, 2267–2270; *Angew. Chem. Int. Ed.* **2002**, *41*, 2163–2166.

[7] F. Gao, Q. Y. Lu, S. H. Xie, D. Y. Zhao, *Adv. Mater.* **2002**, *14*, 1537–1540.

[8] a) X. W. Lou, H. C. Zeng, *J. Am. Chem. Soc.* **2003**, *125*, 2697–2704; b) J. B. Liang, J. W. Liu, Q. Xie, S. Bai, W. C. Yu, Y. T. Qian, *J. Phys. Chem. B* **2005**, *109*, 9463–9467; c) M. S. Mo, J. C. Yu, L. Z. Zhang, S. K. A. Li, *Adv. Mater.* **2005**, *17*, 756–760; d) X. S. Fang, C. H. Ye, L. D. Zhang, J. X. Zhang, J. W. Zhao, P. Yan, *Small* **2005**, *1*, 422–428.

[9] a) Y. W. Jun, S. M. Lee, N. J. Kang, J. Cheon, *J. Am. Chem. Soc.* **2001**, *123*, 5150–5151; b) Z. Wu, C. Pan, T. Li, G. Yang, Y. Xie, *Cryst. Growth Des.* **2007**, *7*, 2454–2459.

[10] a) Z. P. Zhang, X. Q. Shao, H. D. Yu, Y. B. Wang, M. Y. Han, *Chem. Mater.* **2005**, *17*, 332–336; b) C. Coudun, J. F. Hochepicd, *J. Phys. Chem. B* **2005**, *109*, 6069–6074; c) L. X. Yang, Y. J. Zhu, H. Tong, W. W. Wang, *Cryst. Growth Des.* **2007**, *7*, 2716–2719; d) M. H. Cao, X. Y. He, J. Chen, C. W. Hu, *Cryst. Growth Des.* **2007**, *7*, 170–174; e) L. X. Yang, Y. J. Zhu, L. Li, L. Zhang, H. Tong, W. W. Wang, G. F. Cheng, J. F. Zhu, *Eur. J. Inorg. Chem.* **2006**, 4787–4792.

[11] a) L. S. Zhang, W. Z. Wang, L. Zhou, H. L. Xu, *Small* **2007**, *3*, 1618–1625; b) Y. Y. Li, J. P. Liu, X. T. Huang, G. Y. Li, *Cryst. Growth Des.* **2007**, *7*, 1350–1355; c) J. Y. Chen, T. Herricks, M. Geissler, Y. N. Xia, *J. Am. Chem. Soc.* **2004**, *126*, 10854–10885; d) Q. Zhang, W. T. Yao, X. Y. Chen, L. W. Zhu, Y. B. Fu, G. B. Zhang, L. S. Sheng, S. H. Yu, *Cryst. Growth Des.* **2007**, *7*, 1423–1431; e) S. H. Yu, H. Cölfen, A. W. Xu, W. F. Dong, *Cryst. Growth Des.* **2004**, *4*, 33–37; f) T. X. Wang, M. Antonietti, H. Cölfen, *Chem. Eur. J.* **2006**, *12*, 5722–5730; g) Y. Ding, S. H. Yu, C. Liu, Z. A. Zang, *Chem. Eur. J.* **2007**, *13*,

746–753; h) J. Yang, C. X. Li, X. M. Zhang, Z. W. Quan, C. M. Zhang, J. Lin, *Chem. Eur. J.* **2008**, *14*, 4336–4345.
[12] a) Z. M. Fang, Q. Hong, Z. H. Zhou, S. J. Dai, W. Z. Weng, H. L. Wan, *Catal. Lett.* **1999**, *61*, 39–44; b) M. V. Martínez-Huerta, J. M. Coronado, M. Fernández-García, A. Iglesias-Juez, G. Deo, J. L. G. Fierro, M. A. Banãres, *J. Catal.* **2004**, *225*, 240–248.
[13] Y. Terada, K. Shimamura, V. V. Kochurikhin, L. V. Barashov, M. A. Ivanov, T. Fukuda, *J. Cryst. Growth* **1996**, *167*, 369–372.
[14] a) R. A. Fields, M. Birnbaum, C. L. Fincher, *Appl. Phys. Lett.* **1987**, *51*, 1885–1886; b) J. R. O'Connor, *Appl. Phys. Lett.* **1966**, 9, 407–409.
[15] a) J. R. Gambino, C. J. Guare, *Nature* **1963**, *198*, 1084–1084; b) J. W. Stouwdam, M. Raudsepp, C. F. van Veggel, *Langmuir* **2005**, *21*, 7003–7008; c) A. Huignard, T. Gacoin, J. P. Boilot, *Chem. Mater.* **2000**, *12*, 1090–1094.
[16] a) C. J. Jia, L. D. Sun, L. P. You, X. C. Jiang, F. Luo, Y. C. Pang, C. H. Yan, *J. Phys. Chem. B* **2005**, *109*, 3284–3290; b) W. L. Fan, S. Y. Sun, S. X. Sun, X. Zhao, *J. Solid State Chem.* **2007**, *180*, 284–290; c) W. L. Fan, S. Y. Sun, Y. X. Bu, S. X. Sun, X. Zhao, *J. Phys. Chem. B* **2006**, *110*, 23247–23254; d) W. L. Fan, W. Zhao, L. P. You, X. Y. Song, W. M. Zhang, H. Y. Yu, S. X. Sun, *J. Solid State Chem.* **2004**, *177*, 4399–4403; e) W. L. Fan, Y. X. Bu, X. Y. Song, S. X. Sun, X. Zhao, *Cryst. Growth Des.* **2007**, *7*, 2361–2366.
[17] a) J. F. Liu, Y. D. Li, *Adv. Mater.* **2007**, *19*, 1118–1122; b) J. F. Liu, Y. D. Li, *J. Mater. Chem.* **2007**, *17*, 1797–1803; c) H. Deng, S. H. Yang, S. Xiao, H. M. Gong, Q. Q. Wang, *J. Am. Chem. Soc.* **2008**, *130*, 2032–2040; d) L. Zhu, J. Y. Li, Q. Li, X. D. Liu, J. Meng, X. Q. Cao, *Nanotechnology* **2007**, *18*, 055604; e) F. Wang, X. J. Xue, X. G. Liu, *Angew. Chem.* **2008**, *120*, 920–923; *Angew. Chem. Int. Ed.* **2008**, *47*, 906–909; f) X. G. Wu, Y. R. Tao, C. Y. Song, C. J. Mao, L. Dong, J. J. Zhu, *J. Phys. Chem. B* **2006**, *110*, 15791–15796.
[18] G. C. Li, K. Chao, H. R. Peng, K. Z. Chen, *J. Phys. Chem. B* **2008**, *112*, 6228–6231.
[19] Z. P. Peng, Y. S. Jiang, Y. H. Song, C. Wang, H. J. Zhang, *Chem. Mater.* **2008**, *20*, 3153–3162.
[20] a) Z. Tang, N. A. Kotov, M. Giersig, *Science* **2002**, *297*, 237–240; b) S. Lin, M. Li, E. Dujardin, C. Girard, S. Mann, *Adv. Mater.* **2005**, *17*, 2553–2559; c) M. Adachi, Y. Murata, J. Takao, J. Jiu, M. Sakamoto, F. Wang, *J. Am. Chem. Soc.* **2004**, *126*, 14943–14949.
[21] B. Liu, H. C. Zeng, *J. Am. Chem. Soc.* **2005**, *127*, 18262–18268.
[22] a) K. S. Cho, D. V. Talapin, W. G. Gaschler, C. B. Murry, *J. Am. Chem. Soc.* **2005**, *127*, 7140–7147; b) X. S. Fang, C. H. Ye, X. S. Peng, Y. H. Wang, Y. C. Wu, L. D. Zhang, *J. Mater. Chem.* **2003**, *13*, 3040–3043; c) X. S. Fang, C. H. Ye, L. D. Zhang, Y. H. Wang, Y. C. Wu, *Adv. Fun. Mater.* **2005**, *15*, 63–68; d) Z. W. Pan, S. Dai, D. B. Beach, D. H. Lownders, *Nano. Lett.* **2003**, *3*, 1279–1284; e) F. Kim, S. Connor, H. Song, T. Kuykendall, P. Yang, *Angew. Chem.* **2004**, *116*, 3759–3763; *Angew. Chem. Int. Ed.* **2004**, *43*, 3673–3677.
[23] A. Huignard, V. Buissette, G. Laurent, T. Gacoin, J. P. Boilot, *Chem. Mater.* **2002**, *14*, 2264–2269.
[24] Z. C. Jiang, R. X. Cai, H. S. Zhang, *Analytical Chemistry of Rare Earth Element*, Science Press, Peking, **2000**, p. 6.

Received: August 19, 2008
Published online: December 15, 2008

